PAPER

Single-Fourier transform based full-bandwidth Fresnel diffraction

IOP Publishing Journal of Optics
J. Opt. **23** (2021) 035604 (6pp) https://doi.org/10.1088/2040-8986/abdf68

Single-Fourier transform based full-bandwidth Fresnel diffraction

Wenhui Zhang, Hao Zhang and Guofan Jin

State Key Laboratory of Precision Measurement Technology and Instruments, Department of Precision Instrument, Tsinghua University, Beijing 100084, People's Republic of China

E-mail: haozhang274@tsinghua.edu.cn

Received 9 November 2020, revised 4 January 2021
Accepted for publication 25 January 2021
Published 18 February 2021

Abstract

In physical optics, Fresnel diffraction matters. The single Fourier transform method has been widely used in Fresnel diffraction calculation and can perform the direct computation of the output field with high efficiency. Based on a phase-space analysis, we find that the conventional single Fourier transform method cannot correctly deal with the full bandwidth of the input field. Aliasing occurs with high-frequency components because the bandwidth transfer capacity of the conventional method is insufficient, which greatly deteriorates the calculation accuracy. To address this serious problem, we propose a single Fourier transform-based full-bandwidth Fresnel diffraction calculation method. By rearrangement of the sampling resources, all the frequency components can be correctly transferred for accurate, efficient, and flexible Fresnel diffraction calculation.

Keywords: Fresnel diffraction, full-bandwidth transform, phase-space analysis

(Some figures may appear in colour only in the online journal)

1. Introduction

Fresnel diffraction plays an important role in physical optics [1, 2]. Various fast calculation methods have been proposed to quantitatively describe Fresnel diffraction [2–4], which can be roughly divided into two categories: the single Fourier transform method and convolution-based methods. For the single Fourier transform method, only one Fourier transform is used to calculate the Fresnel diffraction; the sampling interval and sampling range of the output field vary with the propagation distance [3]. If the complex amplitude of the output field is of interest, the single Fourier transform method can only be used at one specific distance; and if only the amplitude is of interest, it can be used in far fields [3, 5]. For the convolution-based methods, the sampling interval and sampling range of the output field are the same as those of the input field, and do not vary with the propagation distance [3]. Depending on whether the transfer function or the impulse response function is used, different convolution-based methods have different applicable distance ranges [3, 6]. Due to the differences in sampling properties caused by different implementations, the single Fourier transform method and convolution-based methods can be used in different applications. The single Fourier transform method is popular for applications where the sampling range and interval of the output field are different from those of the input field, such as Fresnel holographic imaging [7, 8] and display [9], holographic projection [10, 11] and computational imaging [12, 13], etc. Similarly, the convolution-based methods have some corresponding applications based on their sampling properties, such as those described in [14–17]. Also, analytical Fresnel diffraction is used in some applications, such as those described in [18, 19].

For these two types of diffraction calculation method, a lot of analysis work has been done to study their properties and application scopes, such as [3, 4, 20, 21]. For the convolution-based methods, the analyses have mainly focused on the sampling of propagation kernels. The band-limited [22] and band-extended methods [23] were proposed to ensure the sampling correctness of the propagation kernels. For single Fourier transform Fresnel diffraction, the analyses mainly focused on the sampling of chirp functions [3]. A band-limited method [21] was proposed for shifted Fresnel diffraction [24] to reduce the aliasing error in the near-field diffraction calculation. A physical analysis associated with the spatial

and spatial frequency extent of the input field was also conducted [20]. In our recent study [4], we noticed that only considering the sampling of chirp functions in single Fourier transform Fresnel diffraction is not rigorous, but an approximation. After careful study, it was found that such an operation could even cause errors in the calculation. Therefore, we finish and submit this paper to report this serious problem and provide our solutions to the community.

In this work, we mathematically analyze this serious problem with the help of phase-space diagrams, and to solve it, we propose a single Fourier transform-based full-bandwidth Fresnel diffraction calculation method. A simple, generalized, and effective rearrangement of the sampling resources is introduced for the product of the input field and the chirp function, which guarantees the correct transfer of all the frequency components for an accurate diffraction calculation. Such a strategy makes the single Fourier transform-based Fresnel diffraction complete as an accurate diffraction calculation method. Meanwhile, the computational efficiency is high and the space-bandwidth product (SBP) of the output field can be flexibly adjusted, benefitting from the used non-uniform fast Fourier transform (NUFFT).

2. SBP evolution of the input field and the sampling requirement analysis

For a given input field $u_i(x)$, the output field $u_o(X)$ after Fresnel diffraction can be expressed, in the form of a single Fourier transform, as

$$u_o(X) = \exp\left(\frac{ik}{2z}X^2\right)\int u_i(x)\exp\left(\frac{ik}{2z}x^2\right)\exp\left(-\frac{ik}{z}Xx\right)\mathrm{d}x \tag{1}$$

where $k = 2\pi/\lambda$ is the wavenumber, λ is the illumination wavelength, z is the propagation distance, and the constants are neglected. Based on equation (1), the output field $u_o(X)$ is the product of the outer chirp function $\exp[ikX^2/(2z)]$ and the Fourier transform of $u_i(x)\exp[ikx^2/(2z)]$, which is the product of the input field and the inner chirp function. Conventionally, only the sampling requirements of these two chirp functions have been considered, and not the products. However, even if the sampling of the inner chirp function $\exp[ikx^2/(2z)]$ is correct, the product $u_i(x)\exp[ikx^2/(2z)]$ may be aliased because the bandwidth of the product is larger than that of the inner chirp function [4, 25]. By beginning with an aliased input, errors will finally appear in the calculated result.

Figure 1 is shown to intuitively illustrate the SBP evolution of the input field $u_i(x)$ in the form of a phase-space diagram to help accurately determine the sampling requirement of each step. In terms of discrete computation, suppose the input field $u_i(x)$ is sampled by N points with an interval Δ_i. Its SBP can then be expressed as a rectangle, as shown in figure 1(a), with $B_f = 1/\Delta_i$ and $L_x = N\Delta_i$, where B_f is the bandwidth and L_x is the spatial extent. Therefore, we have $B_f L_x = N$ points to sample the input field. The rectangle is an upper bound of

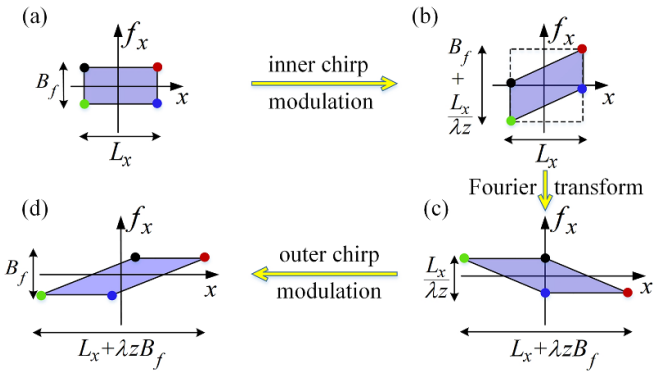

Figure 1. SBP evolution of the input field $u_i(x)$ after each step is shown as a phase-space diagram. B_f and L_x denote the bandwidth and spatial extent of $u_i(x)$, respectively.

the SBP and any geometry is possible inside the rectangle. Because the signal is not known in advance, we use the upper bound to ensure a robust calculation. Note that the replicas [26] are not shown and we expect that their influences on the final result can be avoided by choosing appropriate sampling parameters. After multiplication by the inner chirp function, the bandwidth increases to $B_f + L_x/(\lambda z)$; therefore, we need $[B_f + L_x/(\lambda z)]L_x = N + (N\Delta_i)^2/(\lambda z)$ points to sample it, as indicated by the dashed rectangle in figure 1(b) [4]. The points required are more than we have. Thus, aliasing errors will appear with high-frequency components, due to insufficient bandwidth transfer. In other words, the sampling interval Δ_i can no longer meet the sampling requirement after the bandwidth is increased. In the following, we mathematically analyze and numerically verify this effect.

A necessary condition for sampling $u_i(x)\exp[ikx^2/(2z)]$ correctly is to ensure the sampling correctness of $\exp[ikx^2/(2z)]$. By applying the sampling theorem to it, we have

$$\frac{1}{2\pi}\left|\frac{\partial\varphi(x)}{\partial x}\right|_{\max} \le \frac{1}{2\Delta_i}, \tag{2}$$

where

$$\varphi(x) = \frac{kx^2}{2z} \tag{3}$$

is the phase kernel of $\exp[ikx^2/(2z)]$.

We can get

$$z \ge \frac{N\Delta_i^2}{\lambda}, \tag{4}$$

which means that the inner chirp function $\exp[ikx^2/(2z)]$ can only be sampled correctly within this distance range. Under this condition, we consider the sampling of $u_i(x)\exp[ikx^2/(2z)]$. Its highest spatial frequency [half the bandwidth shown in figure 1(b)] should be no more than half the sampling rate, which is

$$\frac{1}{2}\left(\frac{1}{\Delta_i} + \frac{N\Delta_i}{\lambda z}\right) \le \frac{1}{2\Delta_i}. \tag{5}$$

Table 1. Input fields and the simulation parameters.

Input field	Case I	Case II
Expression	$\mathrm{rect}\,(x/1.6)$	$\cos\left(150\pi x^2\right)\cos\left(0.4\pi x\right)$
Parameters	$\lambda = 500$ nm, $N = 1000$, $\Delta_i = 2$ μm, $z = 10$ mm	

There is no solution to equation (5) unless $N = 0$, because the sampling rate on the right-hand side, determined by Δ_i, is too small, which means that it is impossible to sample the product correctly using the conventional method [27]. The reason no obvious errors have been reported using the conventional method is that the bandwidth of the input field may be far lower than $1/\Delta_i$, or the propagation distance z may be much larger than the size of the input field $N\Delta_i$. In such cases, the reduction in accuracy caused by aliasing errors may be small. However, calculation accuracy cannot be guaranteed in the general case. Readers may notice that under the conditions of equation (4) (which should be satisfied to ensure the sampling correctness of $\exp[ikx^2/(2z)]$), the sampling error of $u_i(x)\exp[ikx^2/(2z)]$ may not be evident. This is not always the case. Only when the propagation distance z is large enough that the term $N\Delta_i/(\lambda z)$ in equation (5) can be ignored, can the sampling correctness of $u_i(x)\exp[ikx^2/(2z)]$ be guaranteed. To show this effect, two numerical demonstrations are carried out. In case I, a rectangular aperture with a width of 1.6 mm is used as the input field. In case II, a cosine-modulated linear chirp grating is used as the object. The analytical expressions of the input fields and all the simulation parameters are listed in table 1.

The calculated amplitude fields are shown in figure 2. We also show the Rayleigh–Sommerfeld integral (RSI) results as [2]. From the comparison, we can see two points: (a) in both of these cases, the accuracy of the result given by the conventional method is affected by the aliasing of the high-frequency components; and (b) the aliasing is more serious for the chirp grating, as shown in the part bounded by the red box, because it has a higher proportion of the high-frequency components. Also, to quantitatively evaluate the calculation accuracy, an signal-to-noise ratio (SNR) metric is used and shown in figure 2, which is defined as

$$\mathrm{SNR} = \frac{\int_s |u(x)|^2 \mathrm{d}x}{\int_s |u(x) - \alpha u_{\mathrm{ref}}(x)|^2 \mathrm{d}x}, \tag{6}$$

where

$$\alpha = \frac{\int\limits_s u(x) u_{\mathrm{ref}}(x) \mathrm{d}x}{\int\limits_s |u_{\mathrm{ref}}(x)|^2 \mathrm{d}x}, \tag{7}$$

$u(x)$ is the amplitude field calculated by the conventional single-FFT Fresnel method, and$u_{\mathrm{ref}}(x)$ is the amplitude field calculated by RSI.

Note that the highest spatial frequency of the cosine-modulated chirp grating is 150 mm^{-1}, which is far from the potential highest spatial frequency $1/(2\Delta_i) = 250$ mm^{-1}.

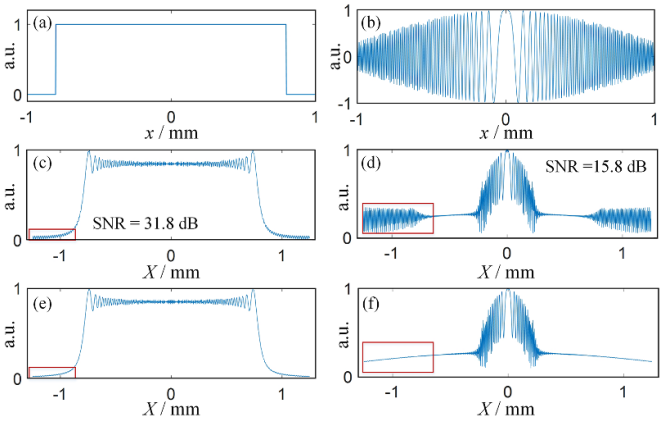

Figure 2. (a) Rectangular aperture; (b) cosine-modulated chirp grating; (c) and (d) are the amplitude fields from the rectangular aperture and the chirp grating obtained using the single-FFT method, respectively; (e) and (f) are the corresponding amplitude fields obtained by RSI.

Despite this, the calculation accuracy is severely impaired due to high-frequency aliasing errors.

3. Single Fourier transform-based full-bandwidth Fresnel diffraction

Since the current sampling interval cannot guarantee full-bandwidth correctness, we can rearrange it. For an input field that has already been sampled with an interval Δ_i (such as a digital hologram recorded by a sensor whose pixel pitch is Δ_i), we can rearrange the sampling interval and use a more densely resampled input field for accurate calculation. Let us revisit equation (5). The reason why there is no meaningful solution is that the sampling rate at the right-hand side is not high enough. To make equation (5) hold, we can use a smaller sampling interval Δ_n during the calculation, which is

$$\frac{1}{2\Delta_i} + \frac{N\Delta_i}{2\lambda z} \leq \frac{1}{2\Delta_n}. \tag{8}$$

This upsampling operation only increases the sampling rate, and does not add any new information about the input field. Thus, the potential highest spatial frequency is still $1/(2\Delta_i)$. On the other hand, because the inner chirp function can only be correctly sampled when $z \geq N\Delta_i^2/\lambda$, the maximum value of the second term on the left-hand side is

$$\max\left\{\frac{N\Delta_i}{2\lambda z}\right\} = \frac{N\Delta_i}{2\lambda}\frac{\lambda}{N\Delta_i^2} = \frac{1}{2\Delta_i}. \tag{9}$$

Substituting equation (9) into equation (8), we get

$$\frac{1}{2\Delta_i} + \frac{N\Delta_i}{2\lambda z} \leqslant \frac{1}{\Delta_i} \leqslant \frac{1}{2\Delta_n}. \tag{10}$$

Therefore, the new sampling interval can be set to

$$\Delta_n = \frac{\Delta_i}{2}. \tag{11}$$

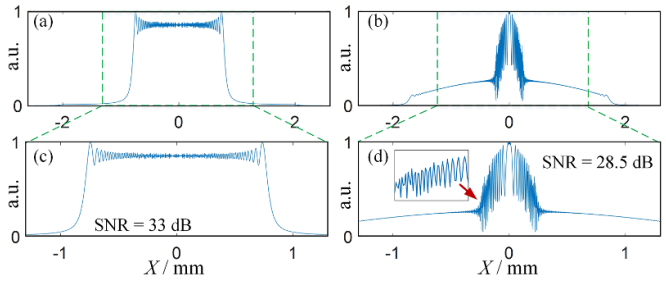

Figure 3. (a) and (b) are the amplitude fields from the rectangular aperture and the chirp grating obtained by the conventional FFT–based method after the upsampling operation, respectively; (c) and (d) are the corresponding zoomed-in regions.

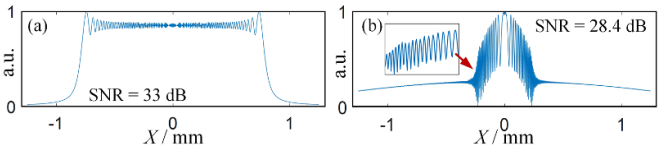

Figure 4. (a) and (b) are the amplitude fields for the rectangular aperture and the cosine-modulated chirp grating obtained using the proposed method, respectively.

The above operation could be summarized as upsampling the Δ_i-sampled input field to be re-sampled by $\Delta_n = \Delta_i/2$. In this work, we use a general approach for this upsampling operation. We first apply FFT to the N-point Δ_i-sampled input field to obtain its Fourier spectrum. We then pad $N/2$ zeros on each side of the spectrum. Finally, we get a $2N$-point $\Delta_i/2$-sampled input field by applying an inverse FFT to the zero-padded spectrum. This operation is equivalent to a sinc interpolation. Because the input size remains constant, the sampling number is doubled, as $N_n = 2N$. That is, the re-sampled input field is sampled by $2N$ points with the interval $\Delta_i/2$, and so is the re-sampled inner chirp function. Thus, $u_i(x)\exp\left[ikx^2/(2z)\right]$ can be correctly sampled within the full bandwidth, as shown in figure 1(b), for accurate calculation. After the correct sampling of $u_i(x)\exp[ikx^2/(2z)]$, which is the prerequisite, the next step is to implement the Fourier transform. However, if the FFT algorithm is used, the output field would be double-sized, as $\lambda z/\Delta_n = 2\lambda z/\Delta_i$. The central part, expressed by N points, is correct, while the parts located at the two sides are wasted, as shown in figure 3. Note that here, 'correctness' should be understood to mean sampling correctness. Because N points just meet the sampling theorem, the resulting output field has a pixelation problem, as indicated by the inset in figure 3, which is more obvious for high-frequency components.

To contribute all $2N$ points for the output field inside the range $\lambda z/\Delta_i$ of the central part, we use another algorithm to implement the Fourier transform, which is called NUFFT. NUFFT is based on FFT and interpolation [28, 29], and is increasingly used in diffraction calculations [23, 30, 31]. In NUFFT, the sampling number and the sampling interval of the transform results can be freely adjusted and are independent of those of the input field. Here, we use type 3 of Greengard and Lee's NUFFT [29], which is defined as

$$P(f_x) = \mathrm{NUFFT}_3\{P(x)\} = \sum_m p(x_m)\exp(-ix_m f_x), \quad (12)$$

where f_x are the spatial frequency locations of the desired Fourier modes; x_m are the sampling point locations of the input field and should be within $[-\pi, \pi)$. Therefore, we first scale the range of x_m from $[-N\Delta_i/2, N\Delta_i/2)$ to $[-\pi, \pi)$ by multiplying by a factor $\tau = 2\pi/(N\Delta_x)$ and then apply NUFFT to $p(x) = u_i(x)\exp[ikx^2/(2z)]$ to obtain $P(f_x)$. Here, we would like to emphasize that we just use NUFFT to redistribute the sampling points in a uniform manner free from the sampling limitations of FFT. NUFFT is just a tool for the flexible allocation of sampling points. The chirp-z transform can also be used [32]. For more details of NUFFT, please see [29].

By comparing equations (1) and (12), we have

$$f_x = \frac{X}{\lambda z}, \quad (13)$$

where $X \in [-L/2, L/2)$ and L is the spatial extent of the output field. Therefore, we can adjust f_x by changing L. Since the output field of interest is inside the range $[-\lambda z/(2\Delta_i), \lambda z/(2\Delta_i))$, the range of f_x in equation (12) is $[-1/(2\Delta_i), 1/(2\Delta_i))$. With this method, the sampling interval of the output field is $\Delta_o = \lambda z/(2N\Delta_i)$. Thus, the sampling points are uniformly distributed in the range $[-\lambda z/(2\Delta_i), \lambda z/(2\Delta_i))$ with an interval of $\lambda z/(2N\Delta_i)$. Figure 4 shows the diffraction amplitude fields obtained by the proposed method, where the output field is smoother and there is no longer a pixelation problem. Readers may ask: since there is pixelation, why does the result given by FFT, shown in figure 3(d), have a high SNR? The answer is that the reference RSI result is also sampled by N points in that case, where there is also pixelation.

All the above analyses focus on the amplitude field. Furthermore, if the complex amplitude is of interest, what should be correctly sampled is not just the separate Fourier transformation, but its modulated version obtained from the outer chirp function. As indicated in figure 1(d), the bandwidth of the final complex amplitude is $B_f = 1/\Delta_i$, therefore, the sampling interval should be

$$\Delta_o \le \Delta_i. \quad (14)$$

That is to say, to correctly sample the complex amplitude of the output field, the sampling interval should be no larger than that of the input field. This sampling requirement can also be satisfied with NUFFT by freely setting the sampling parameters of the transform. In this way, the sampling requirement of the outer chirp function is no longer the key issue, but that of the final output field matters. To avoid pixelation, we set $\Delta_o = \Delta_i/2$; the results are shown in figure 5.

As we can see from figure 5, most information of the output field is located in the central position. Therefore, it would be better if we could just calculate the region of interest (ROI)

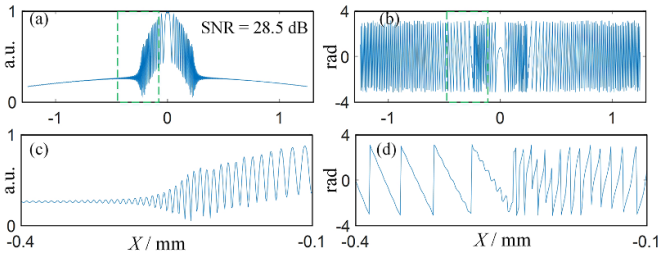

Figure 5. (a) Amplitude field and (b) phase field from the chirp grating obtained by the proposed method [sampled with the interval $\Delta_i/2$]; (c) and (d) are the corresponding zoomed-in parts.

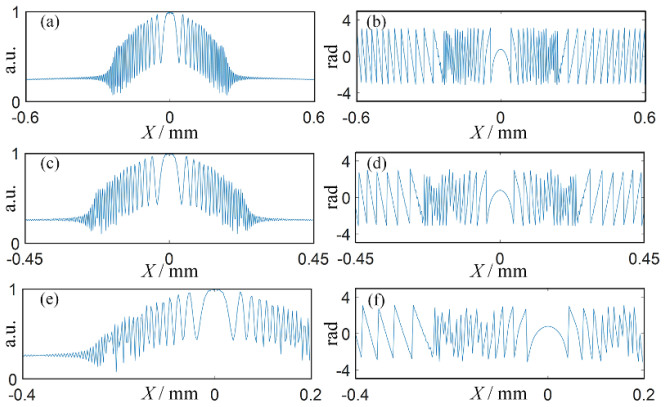

Figure 6. Cases to show the flexible adjustment of the SBP. (a) and (b) are the amplitude and phase within a range of 0.9 mm sampled at intervals of 2 μm, respectively; (c) and (d) are the amplitude and phase within a range of 1.2 mm sampled at intervals of 1.2 μm, respectively; (d) and (e) are the amplitude and phase within $[-0.4, 0.2)$ mm sampled at an interval of 3 μm, respectively.

located in the central area. In other words, it is highly desirable to be able to freely adjust the calculated SBP. Fortunately, with the proposed method, this can be achieved by flexibly adjusting the sampling parameters of the output field. Suppose the range of the ROI is $X \in [-L/2, L/2)$, the highest spatial frequency of the complex amplitude is

$$f_{x\max} = \frac{L}{2\lambda z}. \tag{15}$$

Therefore, the sampling interval is given by the sampling theorem as

$$\Delta_o = \frac{1}{2f_{x\max}} = \frac{\lambda z}{L}. \tag{16}$$

The sampling interval Δ_o becomes larger with a reduced ROI size, which is consistent with the fact that a smaller spatial frequency corresponds to a lower sampling rate. Of course, the sampling interval Δ_o can be flexibly scaled within the range of correct sampling. In figure 6, two calculation cases, $L = 0.9$ mm and 1.2 mm, are presented with the parameters listed in table 1. The sampling intervals, Δ_o, are 2 μm, and 1.2 μm, respectively. From figure 6, it is evident that the proposed

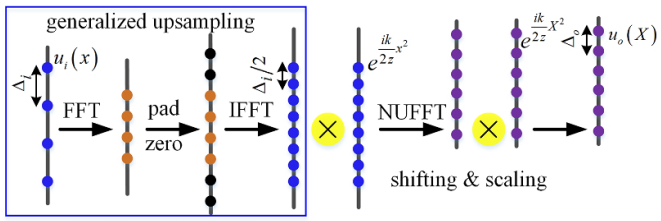

Figure 7. Flowchart of the proposed method.

method can freely adjust the SBP and the sampling parameters of the output field. Note that shifting is also possible just by making $X \in [X_1, X_2)$ asymmetric with the origin, as shown in figures 6(e) and (f) where $\Delta_o = 3$ μm, $X_1 = -0.4$ mm and $X_2 = 0.2$ mm.

4. Discussions and conclusions

We would like to draw the reader's attention to several points. First, the computational complexity of the used NUFFT is O(Nlog$N$), which is comparable to the complexity of an FFT [28]. Thus, the calculation is efficient. Compared with the conventional method, because one FFT and one inverse FFT are added and zero padding is implemented for the Fourier spectrum of the input field, more sampling points are used in the proposed method. Fortunately, because the FFT algorithm is efficient, the calculation time of the proposed method (~70 ms) is comparable with that of the conventional method (~10 ms). Both are on the order of 10 ms with a commercial laptop (CPU 2.9 GHz). The increased sampling points, compared to the conventional FFT–based method are used to guarantee the calculation accuracy of the proposed method, as indicated in the flowchart in figure 7. Second, more points are needed to correctly sample a complex amplitude than a pure amplitude, which means the former has a larger bandwidth. Finally, it is worth mentioning that the proposed method starts from discrete sampling parameters, not the analytical input field [20]. The sampling interval is already given and not determined by the SBP of the input field. Therefore, we need to numerically narrow down the sampling interval for the correct calculation.

To summarize, we have proposed a single Fourier transform-based full-bandwidth Fresnel diffraction calculation method. It has been proven that zero padding in the spatial frequency domain is needed for the single Fourier transform method. The serious problem of high-frequency aliasing in the conventional method, due to insufficient bandwidth transfer, has been analyzed and solved. All the frequency components can be correctly transferred during the calculation by a simple, generalized, and effective upsampling method. With the proposed method, the SBP and sampling parameters of the output field can be freely adjusted, which would benefit multiple applications requiring high calculation accuracy and flexibility, such as holography and diffractive optics. Demo Matlab code for the proposed method can be found in [33].

Acknowledgments

We acknowledge the National Natural Science Foundation of China (NSFC) (62035003, 61875105).

Conflict of interest

The authors declare no conflicts of interest.

ORCID iDs

Wenhui Zhang https://orcid.org/0000-0002-9459-8685
Hao Zhang https://orcid.org/0000-0001-9786-5008

References

[1] Born M and Wolf E 2013 *Principles of Optics: Electromagnetic Theory of Propagation, Interference and Diffraction of Light* (Amsterdam: Elsevier)
[2] Goodman J W 2017 *Introduction to Fourier Optics* (New York: W. H. Freeman)
[3] Voelz D G and Roggemann M C 2009 Digital simulation of scalar optical diffraction: revisiting chirp function sampling criteria and consequences *Appl. Opt.* **48** 6132–42
[4] Zhang W, Zhang H, Sheppard C J R and Jin G 2020 Analysis of numerical diffraction calculation methods: from the perspective of phase space optics and the sampling theorem *J. Opt. Soc. Am.* A **37** 1748–66
[5] Mas D, Garcia J, Ferreira C, Bernardo L M and Marinho F 1999 Fast algorithms for free-space diffraction patterns calculation *Opt. Commun.* **164** 233–45
[6] Mendlovic D, Zalevsky Z and Konforti N 1997 Computation considerations and fast algorithms for calculating the diffraction integral *J. Mod. Opt.* **44** 407–14
[7] Zhang F, Yamaguchi I and Yaroslavsky L P 2004 Algorithm for reconstruction of digital holograms with adjustable magnification *Opt. Lett.* **29** 1668–70
[8] Picart P and Leval J 2008 General theoretical formulation of image formation in digital Fresnel holography *J. Opt. Soc. Am.* A **25** 1744–61
[9] Zhang H, Zhao Y, Cao L and Jin G 2016 Layered holographic stereogram based on inverse Fresnel diffraction *Appl. Opt.* **55** A154–9
[10] Qu W, Gu H, Zhang H and Tan Q 2015 Image magnification in lensless holographic projection using double-sampling Fresnel diffraction *Appl. Opt.* **54** 10018–21
[11] Chang C, Qi Y, Wu J, Xia J and Nie S 2017 Speckle reduced lensless holographic projection from phase-only computer-generated hologram *Opt. Express* **25** 6568–80
[12] Zhang F, Pedrini G and Osten W 2007 Phase retrieval of arbitrary complex-valued fields through aperture-plane modulation *Phys. Rev.* A **75** 043805
[13] Shang Y, Wang X, Sun W, Han P, Ye J, Feng S and Zhang Y 2019 Terahertz image reconstruction based on compressed sensing and inverse Fresnel diffraction *Opt. Express* **27** 14725–35
[14] Zhang W, Cao L, Jin G and Brady D 2018 Full field-of-view digital lens-free holography for weak-scattering objects based on grating modulation *Appl. Opt.* **57** A164–71
[15] Zhang W, Cao L, Brady D J, Zhang H, Cang J, Zhang H and Jin G 2018 Twin-image-free holography: a compressive sensing approach *Phys. Rev. Lett.* **121** 093902
[16] Zhang H, Cao L and Jin G 2017 Computer-generated hologram with occlusion effect using layer-based processing *Appl. Opt.* **56** F138–43
[17] Zhang H, Cao L and Jin G 2019 Three-dimensional computer-generated hologram with Fourier domain segmentation *Opt. Express* **27** 11689–97
[18] Ebrahimi S and Dashtdar M 2019 Quantitative phase imaging based on Fresnel diffraction from a phase plate *Appl. Phys. Lett.* **115** 203702
[19] Hooshmand-Ziafi H, Dashtdar M and Hassani K 2020 Measurement of the full complex degree of coherence using Fresnel diffraction from a phase discontinuity *Opt. Lett.* **45** 3737–40
[20] Kelly D P 2014 Numerical calculation of the Fresnel transform *J. Opt. Soc. Am.* A **31** 755–64
[21] Shimobaba T, Kakue T, Okada N, Oikawa M, Yamaguchi Y and Ito T 2013 Aliasing-reduced Fresnel diffraction with scale and shift operations *J. Opt.* **15** 075405
[22] Matsushima K and Shimobaba T 2009 Band-limited angular spectrum method for numerical simulation of free-space propagation in far and near fields *Opt. Express* **17** 19662–73
[23] Zhang W, Zhang H and Jin G 2020 Band-extended angular spectrum method for accurate diffraction calculation in a wide propagation range *Opt. Lett.* **45** 1543–6
[24] Muffoletto R P, Tyler J M and Tohline J E 2007 Shifted Fresnel diffraction for computational holography *Opt. Express* **15** 5631–40
[25] Hennelly B M and Sheridan J T 2005 Generalizing, optimizing, and inventing numerical algorithms for the fractional Fourier, Fresnel, and linear canonical transforms *J. Opt. Soc. Am.* A **22** 917–27
[26] Hennelly B M, Healy J J and Sheridan J T 2010 Sampling in phase space *Phase-Space Optics Fundamentals and Applications* ed M E Testorf, B M Hennelly and J Ojeda-Castaneda (New York: McGrawHill) pp 309–36
[27] Zhang W, Zhang H and Jin G 2020 Frequency sampling strategy for numerical diffraction calculation *Opt. Express* **28** 39916–32
[28] Greengard L and Lee J-Y 2004 Accelerating the nonuniform fast Fourier transform *SIAM Rev.* **46** 443–54
[29] Lee J-Y and Greengard L 2005 The type 3 nonuniform FFT and its applications *J. Comput. Phys.* **206** 1–5
[30] Zhang W, Zhang H and Jin G 2020 Adaptive-sampling angular spectrum method with full utilization of space-bandwidth product *Opt. Lett.* **45** 4416–9
[31] Shimobaba T, Matsushima K, Kakue T, Masuda N and Ito T 2012 Scaled angular spectrum method *Opt. Lett.* **37** 4128–30
[32] Rabiner L, Schafer R and Rader C 1969 The chirp z-transform algorithm *IEEE Trans. Audio Electroacoust.* **17** 86–92
[33] Zhang W, Zhang H and Jin G 2020 Single-Fourier transform based full bandwidth Fresnel diffraction (available at: https://github.com/thu12zwh/Single-Fourier-transform-based-full-bandwidth-Fresnel-diffraction)